SYSTEM-LEVEL DESIGN OF CENTRALIZED THERMAL AND ELECTRICAL NETWORKS FOR A NET-ZERO VIRTUAL CAMPUS IN MONTREAL

Haas Maxime[1], Cabay Raphaël[2], Werbrouck Alexis[2], O.Hamad Ishak[2]

[1] Civil Engineer in Energy Engineering, Specialising in Energy Conversion, University of Liège

[2] Civil engineer in energy engineering, Specialising in Energy Networks, University of Liège

Abstract

This study proposes the design of a net-zero energy campus in Montreal powered entirely by local renewable resources, including photovoltaic panels, wind turbines, a biomass unit, and a run-of-river hydroelectric plant. A centralized thermal network with a four-pipe heat pump system meets both heating and cooling needs, operating with high thermodynamic efficiency and converting thermal loads into equivalent electrical demand. A full thermoelectric load assessment and network optimization were performed. The total capital cost for the thermal network, including generation and piping infrastructure, estimated at approximately 4 M€ with annual operating costs around 458 k€. The electrical network, modeled through a mixed-integer non-linear optimization framework, approximates annualized cost over 20 years at 240 k€/y, while proving technically feasible and economically viable for long-term sustainable development.

Keywords. Zero-Energy Campus, 4-pipe Heat Pump, Energy Mix, District Heating, Grid Optimisation.

Nomenclature

V	Volume [m^3]
u	Wind speed [m/s]
σ_u	Standard deviation of wind speed [m/s]
ρ	Density [kg/m^3]
η	Efficiency [–]
TI	Turbulence Intensity [–]
WDP	Wind Power Density [W/m^2]
S	Surface area [m^2]
T	Temperature [°C]
E	Energy [MWh]
$\dot{W}/\dot{Q}$	Power/Thermal power [MW]
TER	Thermal Efficiency Ratio [–]
TFO	Transmission Feed-Out [–]
HV/MV/LV	High/Medium/Low Voltage [V]
t	Time step subscript
TPIC	Total Pipe Infrastructure Cost [€]
COC/COH	Cost of Cold/Heat [€/MWh]
4P-HP	Four-pipe Heat Pump [–]
$\dot{m}$	Mass flow rate [kg/s]
AU	Heat transfer coefficient [W/K]
p	Pressure [Pa]
h	Enthalpy [J/kg K]
U	Voltage [V]
I	Electric current [A]
$\dot{V}$	Volumetric flow rate [m^3/s]
P/Q	Active/Reactive power [W/VAR]
$d \in \{1,2,3\}$	Representative days subscript
$\mathrm{ch}, \mathrm{dis}$	Charge and Discharge supscripts
Se	State of charge of a storage unit
AS	Apparent power [VA]

1 Introduction

The novel challenges posed by global warming, the rise of microgrids, and the use of green energy are driving research into net zero-energy campuses, with a strong emphasis on renewables. In this context, the present study introduces a case study of a renewable campus that produces all its energy on-site in Montreal. Achieving this goal requires drawing upon insights from previous studies. For example, Los Angeles Community College has focused on developing photovoltaic energy, installing 4.21 MW of capacity to move toward a net zero-energy campus [1]. The University of Applied Sciences in Stuttgart aims to cut CO_2 emissions by enhancing energy efficiency and integrating renewables. Key strategies include retrofitting buildings and deploying a district heating system with heat pumps, photovoltaic panels, and CHP units [2]. The University of Valladolid uses a biomass-based district heating system combined with real-time energy monitoring [3]. Morris University is working toward zero energy consumption through large wind turbines meeting up to 60% of demand, along with solar thermal systems for heating [4]. At the University of Liege, a 9 M€ biomass cogeneration system was integrated into the existing thermal plant, supplying a 24 km district heating network. Fueled by 16 300 tonnes of wood pellets annually, the system reduces CO_2 emissions by up to two-thirds of the plant's output, and meets 70% of the campus's heat needs and

30% of its electricity demand [5].

In all cases, the technology employed is adapted upon the geographical location and prevailing climatic conditions of the campus. Consequently, this approach must also be adopted. The primary objective of this paper is to explore the potential for the campus to generate a net positive amount of energy, thereby achieving a zero-energy status. This approach is intended to minimise CO_2 emissions by leveraging renewable energy sources and promoting sustainable practices.

The present paper is divided into four sections. Section 2 explores the constraints and opportunities associated with the Montreal campus. Section 3 then addresses the infrastructure and technologies of the thermal grid for the centralized system. Section 4 provides an overview of the potential energy mix for the campus. Finally, Section 5 discusses the infrastructure and technologies of the electrical grid.

2 Constraints and Opportunities of the Montreal Campus

This section outlines the spatial layout, energy needs, and natural resources of the Montreal campus. It assesses demand profiles and topography for storage to inform system design.

2.1 Campus Structure

The campus covers 500 ha and is divided into four districts, named Dupéré, Hochelaga, Overdale and Anjou, each containing between 7 and 11 buildings. Figure 1 shows their layout and interconnecting roads.

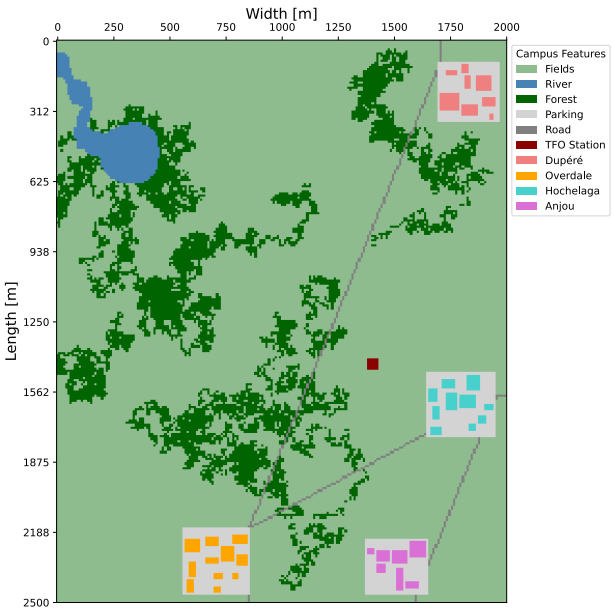

Figure 1: Map of the four campus districts and main roads.

The detailed interactive map is available here.

Building types range from flats and hospitals to hotels, offices, restaurants, schools, warehouses and retail strip malls. Sizes vary from 7200 m² (7 floors) down to 900 m² (1 floor).

A lake fed by a river sits at the campus's lowest point and lies 200 m below the highest elevation; this topographical feature offers potential for energy storage. The campus also benefits from abundant open land and rooftop area. These natural resources will be evaluated for energy integration in Section 4.

2.2 Energy Demand Overview

The campus's annual heating and cooling demands are shown in Figure 2. Cooling consumption significantly exceeds heating, largely driven by continuous chiller operation in hospitals, hotels and restaurants and by office data-centers. The campus's annual electricity demand is shown in Figure 3.

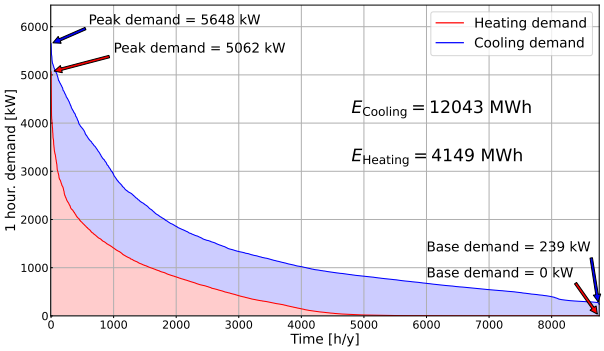

Figure 2: Campus heating and cooling load-duration curve.

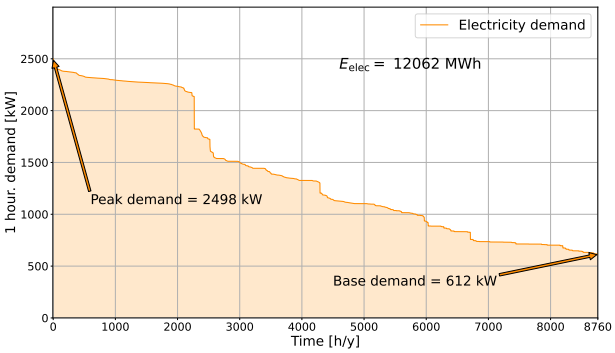

Figure 3: Campus electrical load-duration curve.

3 Thermal District Technologies and Infrastructure

Given the spatial configuration of the Montreal campus, which is divided into four distinct districts and considering its specific energy demands, a centralized system for thermal energy production and distribution is adopted, following the examples of the University of Liège and the University of Valladolid. Unlike these cases, a combined heating and cooling centralized net-

work is designed due to the campus's significant cooling demand. The centralized system is expected to enable optimized management of energy resources, notably through the integration of efficient heat pumps and an adapted distribution infrastructure, ensuring a technically and economically balanced solution.

3.1 Pipe Network Design

To supply heating and cooling to all campus districts, a fully centralized piping network is designed. Four pipelines are required: one supply and one return pipe for heating, and one supply and one return pipe for cooling. These pipelines are routed alongside the existing campus road to minimize excavation costs. All four pipes are laid within the same trench on one side of the road. This results in a total network length of 7.6 km.

Using a numerical model developed by Prof. Dewallef, the optimal pipe radius and the resulting Cost of Heat (COH) and Cost of Cold (COC) are calculated based on thermophysical and economic parameters.

The supply temperatures for both heating and cooling have been selected in accordance with the specifications of the chosen thermal generation system, namely a 4-pipe Heat Pump (4P-HP) unit. This technology is further detailed in the following subsection.

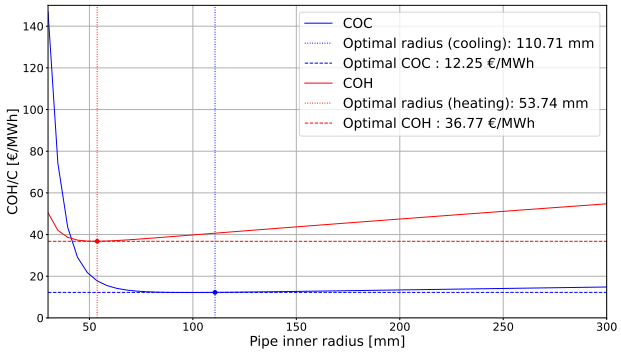

(a) Levelised Cost of Heat and Cold versus pipe inner radius.

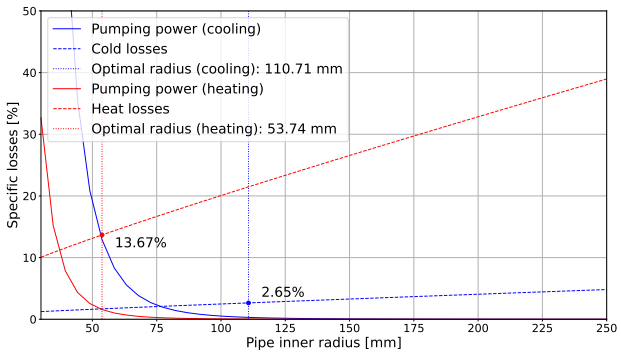

(b) Break-down of specific thermal and pumping losses versus pipe inner radius.

Figure 4: Optimisation of pipe inner radius for the centralized thermal network.

Figures 4a–4b shows how the pipe inner radius influences both the levelised Cost of Heat (COH) and the specific losses (thermal conduction and pumping). The optimum radius minimises the sum of these losses, thereby yielding the lowest COH. The same methodology is applied to the cooling circuit, leading to the optimal values reported below.

- **Heating circuit:** radius $= 53.74$ mm, $\text{COH}_{\text{pipe}} = 36.77$ €/MWh, heat losses $= 13.67\%$
- **Cooling circuit:** radius $= 110.71$ mm, $\text{COC}_{\text{pipe}} = 12.25$ €/MWh, cold losses $= 2.65\%$

Once the optimal pipe dimensions are selected, the thermal losses along the network are quantified and used to update the original heating and cooling demands. This correction reflects the actual amount of energy that must be supplied by the generation systems, accounting for distribution inefficiencies. The heating and cooling demands are increased by 13.7% and 2.7% respectively to account for losses in the distribution circuit. Figure 5 presents the updated heating and cooling load-duration curve.

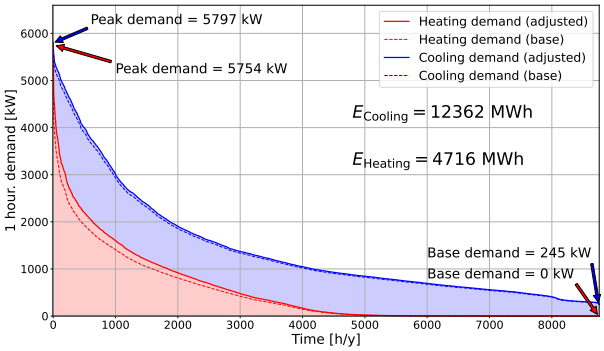

Figure 5: Heating and cooling load-duration curve with loss correction.

Cooling remains the dominant thermal requirement over the year in terms of total energy demand. However, peak loads for heating and cooling are now of comparable magnitude.

The total cost associated with the production and installation of the piping network can be estimated. Specifically, the Total Pipe Infrastructure Cost (TPIC) is defined as:

$$\text{TPIC} = \text{COH}_{\text{pipe}}\, E_{\text{heat}} + \text{COC}_{\text{pipe}}\, E_{\text{cold}} \qquad (1)$$

Based on the estimated heating and cooling demands and associated unit costs, the TPIC is approximately 325 000 €.

3.2 Thermal Centralized Generation System

The analysis of typical weekly heating and cooling demand profiles for each season reveals that simultaneous thermal needs occur throughout most of the year,

with the exception of summer where cooling dominates. This observation is particularly evident during the rest of the year, where significant portions of the campus require both heating and cooling at different times of the day. Typical weekly profiles were generated by computing the average hourly heating and cooling demands for each day of the week, aggregated over all weeks within each season.

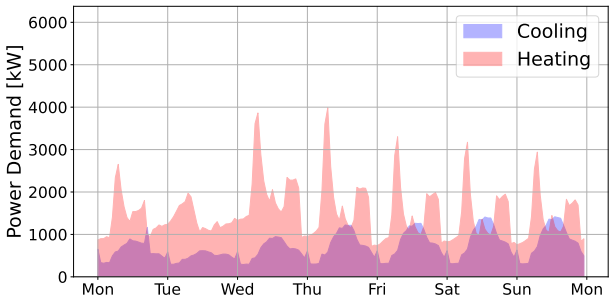

Figure 6: Typical weekly demand in winter (Dec–Feb).

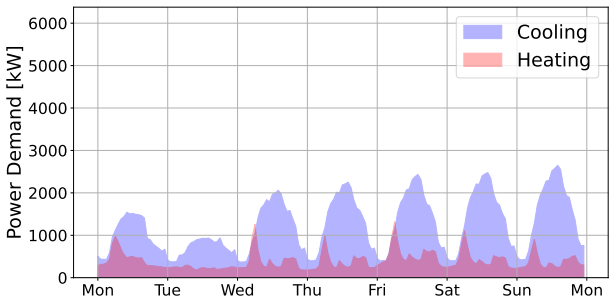

Figure 7: Typical weekly demand in spring (Mar–May).

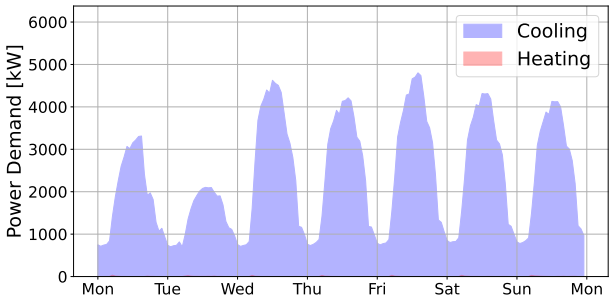

Figure 8: Typical weekly demand in summer (Jun–Aug).

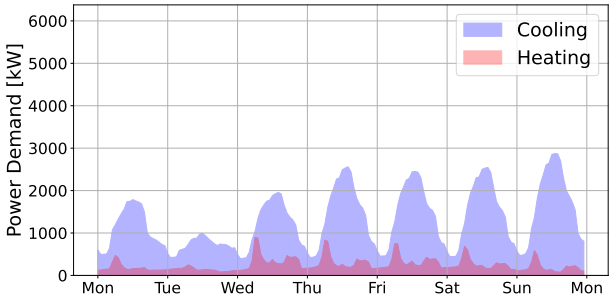

Figure 9: Typical weekly demand in fall (Sep–Nov).

To efficiently address overlapping thermal demands, a centralized 4P-HP system is selected. This technology enables simultaneous heating and cooling production using a shared refrigeration cycle. By reusing rejected heat, the four-pipe configuration improves thermodynamic efficiency and reduces primary energy consumption while ensuring year-round thermal flexibility and minimizing required production units.

The 4P-HP system comprises a central refrigeration cycle and two hydraulic loops. The refrigeration loop includes a compressor, two expansion valves, and two heat exchangers (evaporator and condenser) connected to separate water circuits for simultaneous heating and cooling. An air exchanger (finned coil in Figure 10) integrated into the refrigeration cycle absorbs or rejects surplus heat, ensuring thermal balance when heating and cooling demands are misaligned. Multiple three-way valves regulate flow rates dynamically, enabling energy delivery to both loops based on real-time demand.

A 4P-HP model from FläktGroup (FGAS8080EG2.HE) was identified as suitable for the centralized thermal generation system. Manufacturer performance data for simultaneous heating and cooling are summarised in Table 1.

Table 1: Performance data of the selected 4P-HP (simultaneous heating and cooling mode) at full load [6].

Parameter	Symbol	Value
Cooling capacity	$\dot{Q}_{ev}$	807.2 kW
Heating output	$\dot{Q}_{cd}$	1030 kW
Power consumption	$\dot{W}_{ch}$	241.8 kW
Thermal Efficiency Ratio	TER	7.6
Chilled water outlet T	$T_{w,ex,ev}$	7 °C
Hot water outlet T	$T_{w,ex,cd}$	45 °C

The simplified schematic in Figure 10 is based on the detailed diagram provided by the manufacturer. It is important to note that the specific model selected consists of four such cycles operating in parallel.

For the continuation of the study, the technical documentation provided by the manufacturer contains essential parameters to support the development of a steady-state thermodynamic model using EES (Engineering Equation Solver). This includes information on the refrigerant type, thermodynamic and pressure limits, temperature ranges, electrical characteristics, control logic, and configuration options. Although marked as confidential, both documents (detailed diagram and technical documentation) were shared by FläktGroup upon request within the framework of this academic project.

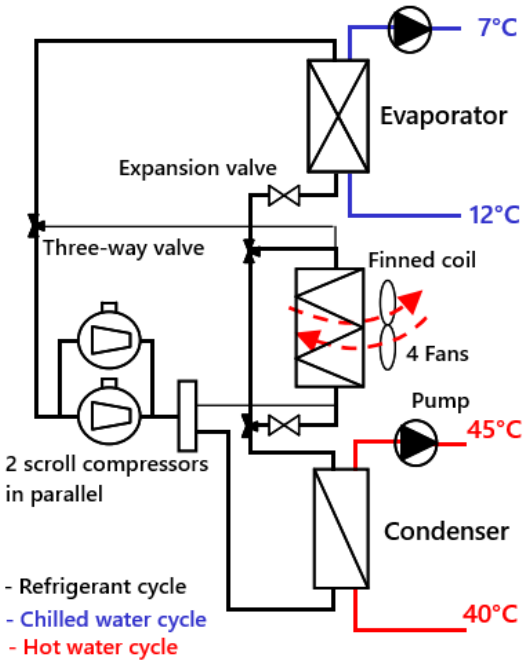

Figure 10: Simplified schematic of a single stage of the selected 4P-HP. Simultaneous heating and cooling are produced from the same refrigeration cycle.

The EES modeling is based on a single-stage refrigeration cycle representation. Since the actual machine consists of four identical modules operating in parallel, the input heating and cooling full load capacities were divided by four, while the Thermal Efficiency Ratio (TER) and operating temperatures were preserved. The water mass flow rates in the two hydraulic cycles are derived from Prof. Dewallef's code, and additional parameters are obtained from the manufacturer's technical documentation. The full load power consumption ($\dot{W}_{ch}$) includes both fans and compressors consumption.

Before the modeling, several assumptions were made to simplify the thermodynamic analysis while maintaining adequate accuracy:

- Steady-state operation with no transient effects
- Refrigerant superheating ($\Delta T_{r,oh}$) of 5 K at the evaporator outlet (compressor inlet)
- Refrigerant subcooling ($\Delta T_{r,sc}$) of 5 K at the condenser outlet
- Adiabatic compression process in the compressor with mechanical losses
- No leakage flux in the compressor
- Isenthalpic expansion through the expansion valve
- Negligible pressure drops in heat exchangers and connecting pipes
- Uniform water temperatures at heat exchanger inlets and outlets

The scroll compressor was modeled using a two-stage compression process to account for the specific characteristics of this technology. The compression work was calculated as the sum of isentropic compression work and constant volume compression work.

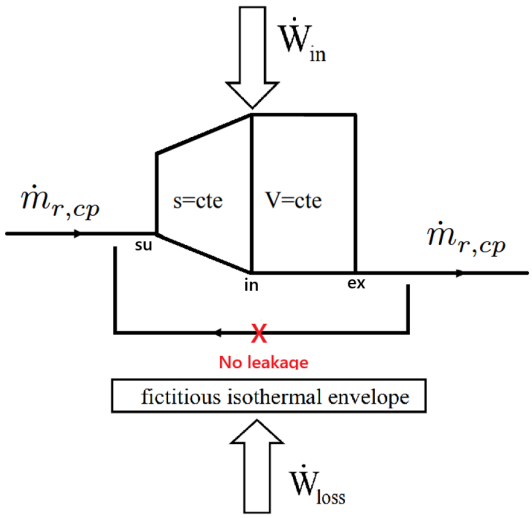

Figure 11: Model of one scroll compressor.

Isentropic compression (suction to intermediate state):

$$\dot{W}_{in,1} = (h_{r,in} - h_{r,su})\ \dot{m}_{r,cp} \tag{2}$$

where $\dot{m}_{r,cd} = \dot{m}_{r,ev} = 2\ \dot{m}_{r,cp}$, due to the two compressors in parallel.

Constant volume compression (intermediate to discharge):

$$\dot{W}_{in,2} = v_{r,in}\ (p_{r,ex} - p_{r,in})\ \dot{m}_{r,cp} \tag{3}$$

where $v_{r,in}$ is the built-in volume ratio of one scroll compressor.

The power consumption of one scroll compressor is given by :

$$\dot{W}_{cp} = \dot{W}_{in} + \dot{W}_{loss} \tag{4}$$

$$= \dot{W}_{loss,0} + (1+\alpha)\ \dot{W}_{in} \tag{5}$$

The power consumption of a single-stage is then :

$$\dot{W}_{ch} = \dot{W}_{cp}\ N_{cp} + \dot{W}_{fan} \tag{6}$$

Due to the predominance of cooling demand in the campus, the fans are considered to operate at full load throughout the year.

Both the evaporator and condenser were modeled using the effectiveness-NTU method.

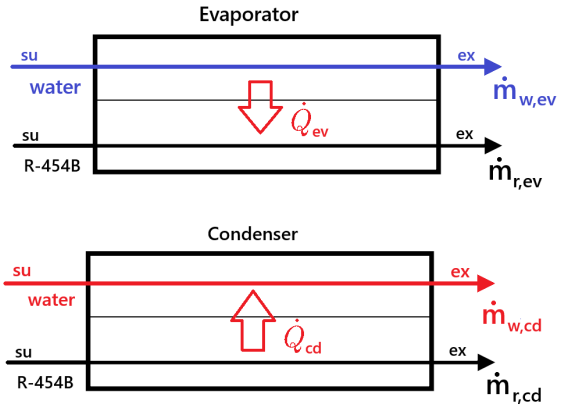

Figure 12: Model of the evaporator and condenser.

The heat transfer effectiveness:

$$\varepsilon_{cd} = 1 - exp\left(-\frac{AU_{cd}}{\dot{C}_{w,cd}}\right) \tag{7}$$

$$\varepsilon_{ev} = 1 - exp\left(-\frac{AU_{ev}}{\dot{C}_{w,ev}}\right) \tag{8}$$

The heat transfer rates are then calculated as:

$$\dot{Q}_{cd} = \varepsilon_{cd}\, \dot{C}_{w,cd}\, (T_{cd} - T_{w,ex,cd}) \tag{9}$$

$$\dot{Q}_{ev} = \varepsilon_{ev}\, \dot{C}_{w,ev}\, (T_{w,su,ev} - T_{ev}) \tag{10}$$

The thermodynamic properties of R-454B refrigerant were calculated using EES built-in property functions. Key state points in the cycle were determined as follows:

Compressor inlet conditions:

- Temperature: $T_{r,su,cp} = T_{r,sat,su} + \Delta T_{r,oh}$
- Pressure: $p_{r,su,cp} = p_{sat}(T_{ev}, x = 0.5)$

Compressor outlet conditions:

- Pressure: $p_{r,ex,cp} = p_{sat}(T_{cd}, x = 0.5)$
- Enthalpy: $h_{r,ex,cp} = h_{r,su,cp} + \frac{\dot{W}_{cp}}{\dot{m}_{r,cp}}$

Condenser outlet conditions:

- Temperature: $T_{r,ex,cd} = T_{r,sat,ex} - \Delta T_{r,sc}$
- Enthalpy: $h_{r,ex,cd} = h(P_{r,ex,cp}, T_{r,ex,cd})$

The TER is given by:

$$\text{TER} = \frac{\dot{Q}_{ev} + \dot{Q}_{cd}}{\dot{W}_{ch}} \tag{11}$$

To calibrate the model, the TER and the power consumption at full load were used as reference points. The parameters in Table 2 were initially guessed and subsequently adjusted iteratively until the model reproduced the target TER value of 7.6 under standard operating conditions. Once the steady-state calibration was completed, a parametric table was implemented to import hourly heating and cooling demands—adjusted to account for thermal distribution losses—enabling an hourly steady-state computation of the TER throughout the year.

The values presented in Table 2 correspond to the final calibrated parameters used in the simulations.

Table 2: Calibrated parameters of the model.

Parameter	Symbol	Value
AU of the condenser	AU_{cd}	60 kW/K
AU of the evaporator	AU_{ev}	90 kW/K
Compressor loss coefficient	α	0.16 kW
Stand-by mechanical loss	$\dot{W}_{loss,0}$	0.93 kW
Built-in volume ratio	$r_{v,in}$	2.7

To better understand the relationship between thermal demands and system efficiency, the hourly TER values were analyzed against the total energy demand for a single refrigeration cycle (representing 1/29th of the total system capacity). This relationship is illustrated in Figure 13.

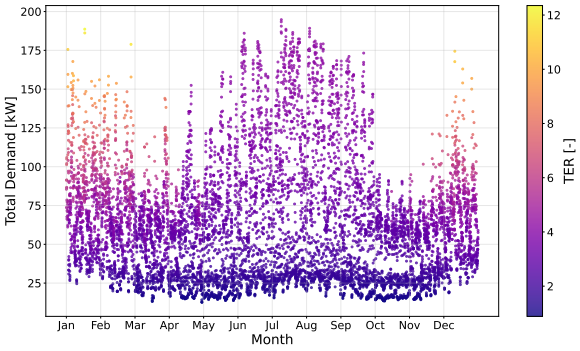

Figure 13: TER versus total thermal demand for one refrigeration cycle throughout the year, showing monthly seasonal patterns.

There is a clear trend showing that TER values increase with higher thermal demands. This behavior is expected as the system operates closer to its nominal design conditions, where it achieves optimal thermodynamic performance. Conversely, the lower TER values correspond to periods of reduced demand—primarily during nighttime hours (represented by darker blue points)—when the system operates at a significantly lower percentage of its design capacity, resulting in reduced efficiency.

More importantly, the analysis demonstrates that winter months achieve higher TER values compared to

summer months, even at similar total demand levels. This enhanced performance during winter is attributed to the more balanced thermal demand profile characteristic of cold seasons, as previously illustrated in Figure 6. During winter, the campus requires approximately equal quantities of heating and cooling, enabling the 4P-HP system to maximize heat recovery and valorize both thermal outputs simultaneously.

In contrast, summer operation is dominated by cooling demand with minimal heating requirements, limiting the system's ability to recover and valorize waste heat. This operational mode results in lower overall efficiency, as only one thermal output is being fully utilized while the heat recovery potential remains largely unexploited.

Since all thermal demands on the campus are met by a centralized 4P-HP system, both heating and cooling loads are entirely supplied by electricity. Therefore, the thermal load-duration curves must be converted into equivalent electrical loads, based on the hourly TER, computed using the calibrated EES model.

For each hour t, the combined thermal demand $\dot{Q}_{\text{th}}(t)$, including both heating and cooling needs corrected for distribution losses, is converted into an equivalent electrical load based on the corresponding TER(t). The resulting quantity, denoted $E_{\text{th,eq}}(t)$, represents the instantaneous electricity required by the 4P-HP to satisfy thermal demands, and is computed as:

$$E_{\text{th,eq}}(t) = \frac{\dot{Q}_{\text{th}}(t)}{\text{TER}(t)} \tag{12}$$

This operation produces an hourly electricity demand profile exclusively attributable to thermal generation. When this profile is added to the non-thermal electricity demand of the campus, the resulting curve reflects the total electrical load required to operate all campus systems. The outcome of this correction can be observed in Figure 14.

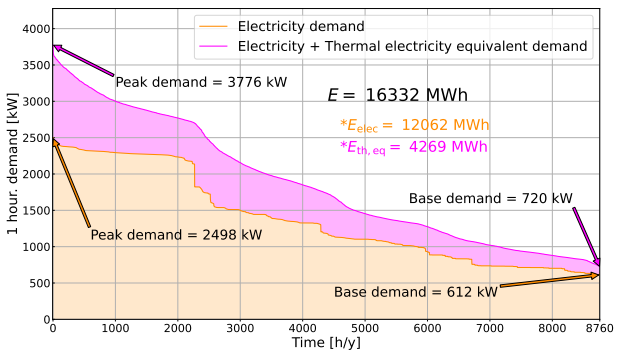

Figure 14: Campus electrical load-duration curve, including direct electricity demand and the additional equivalent electrical demand from thermal needs.

In order to estimate the capital cost of the centralized thermal generation system, manufacturer data for the selected 4P-HP model were used. According to the technical documentation provided by FläktGroup, the unit price of this machine is approximately 500 k€ for a configuration consisting of four parallel refrigeration cycles. This corresponds to a cost of 125 k€ per individual cycle.

To meet the total heating and cooling demand of the campus, a total of 29 refrigeration cycles are required. The resulting construction cost for the complete system is therefore estimated as follows:

$$C_{\text{construction}} = 3.625 \text{ M€} \tag{13}$$

This value accounts for the capital investment related to the equipment alone, and excludes installation, commissioning, or auxiliary infrastructure costs, which may be considered in a more detailed financial assessment.

The total cost of the thermal network is therefore given by:

$$\begin{aligned} \text{Total Cost} &= \text{TPIC} + C_{\text{construction}} \\ &\approx 4 \text{ M€} \end{aligned} \tag{14}$$

In addition to the total cost, operational cost have been assumed to consist solely of electricity costs, while maintenance and other recurring charges are neglected. Based on an annual equivalent electricity consumption of 4.27 GWh and at price of 107.19 €/MWh (the electicity price come from the conclusion of the Section 4), the yearly operating cost is given by :

$$\text{Operational Cost} \approx 458 \text{ k€/y} \tag{15}$$

4 Prospective Energy Mix for the Campus

Various options have been considered for the energy mix to achieve net-zero emissions for the campus. In Quebec, electricity generation is predominantly supplied by hydroelectricity, followed by solar, wind, and biomass energy sources [7]. Initially, the concept was to derive power from the nearest hydroelectric dam directly to the campus. However, depending on hydroelectricity from a 45-km distant dam would not qualify as net zero, since this would require grid-supplied electricity and extensive transmission infrastructure.

A new approach was therefore developed, focusing on local renewable energy generation to create a diversified portfolio while maintaining energy security. This led to exploring the Saint Lawrence River, located just 5 kilometers from the campus, where diverting 1% of

the river's flow could provide local hydroelectric generation. This minimal diversion maintains the river's ecological integrity and remains well below the commonly referenced 10% threshold for environmental degradation [8]. The resulting 25-meter-wide canal would be negligible compared to the Saint Lawrence's 2-kilometer width.

Complementing this local hydro resource, biomass generation was identified as a key non-intermittent alternative within Quebec's renewable energy landscape. Biomass offers carbon neutrality since CO_2 captured by plants during growth offsets emissions released during combustion. In addition, a pumped-storage hydroelectric system will be implemented using the natural elevation difference and lake identified in the campus topography. This system will provide energy buffering capacity, essential for balancing intermittent renewable sources and ensuring supply stability.

This section presents the proposed energy mix for achieving optimal performance and environmental sustainability, followed by the detailed sizing and feasibility assessment of each technology.

4.1 Proposed Energy Mix

The final energy mix incorporates photovoltaic panels (PV), wind turbines, a run-of-river hydroelectric power plant, and biomass generation, complemented by pumped storage utilizing the existing lake. This configuration minimizes renewable energy curtailment while maximizing storage capacity for enhanced operational efficiency. Figure 15 provides a clear and comprehensive illustration of this energy mix composition, considering the actualized load duration curve obtained in Section 3.

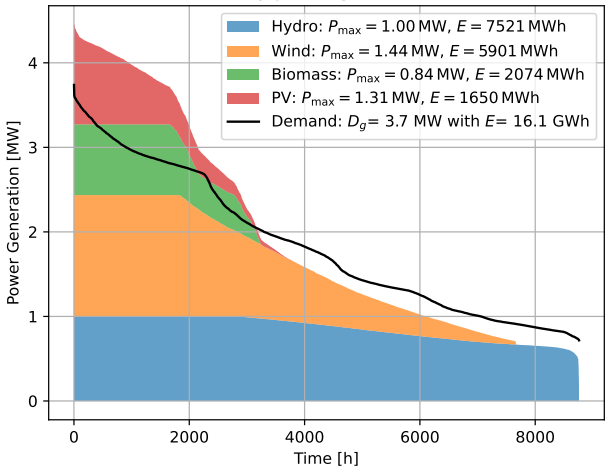

Figure 15: Energy mix for the campus.

This energy mix finds an optimal solution at 107.19 €/MWh with CO_2 emissions at 7.57 kg/MW.

4.2 Run-of-River Hydroelectric

The required hydro power plant has a maximum capacity of 1 MW, which defines the plant's rated size and serves as a key parameter in the economic optimization, since the low marginal cost of hydro generation drives the optimizer to dispatch this resource first whenever the flow allows.

To assess the run-of-river potential on the Saint Lawrence River, hourly flows are estimated by applying a tidal sinusoidal variation to the daily minimum, median and maximum discharges. Diverting 1% of the river flow yields a flow rate ($\dot{V}$) oscillating roughly between 60 m^3/s and 100 m^3/s. Assuming an available head (H) of 2 m and adopting an overall efficiency η=0.5, typical for a small hydro installation, the theoretical hydraulic power is given by:

$$\dot{W} = \rho \, g \, \dot{V} \, H \, \eta \tag{16}$$

The actual instantaneous power therefore ranges between approximately 0.6 MW and 1 MW depending on the flow, providing a maximum potential capacity of 1 MW.

4.3 Wind Power

Before considering wind turbine installation, it is essential to assess the wind resource potential at the Montreal campus. The wind characteristics of the site were evaluated using two key indicators: the Turbulence Intensity (TI) and the Wind Power Density (WPD), defined as:

$$\mathrm{TI} = \frac{\sigma_u}{\overline{u}} \tag{17}$$

$$\mathrm{WPD} = \frac{1}{2} \, \rho_{\mathrm{air}} \, \overline{u^3} \tag{18}$$

Here, σ_u represents the standard deviation of wind speed, and $\overline{u}$ its mean. In this analysis, both were computed over hourly intervals using hourly wind speed values.

For the Montreal site, the annual average turbulence intensity was found to be 0.177, which corresponds to a moderately turbulent environment. The corresponding wind power density was estimated at 272 W/m^2, placing the site within the range of moderate wind resources. Additionally, as shown in Figure 16, the data indicates that wind speed remains within the operational range of a typical wind turbine for approximately 7754 h/y, corresponding to a capacity utilisation of about 88.5%. The wind measurements were taken at 80 m height and the cut-in/cut-out speeds used are aligned with the specifications of the selected wind turbine described further in this section.

Given these favorable conditions, the wind installation is deemed feasible for the Montreal site.

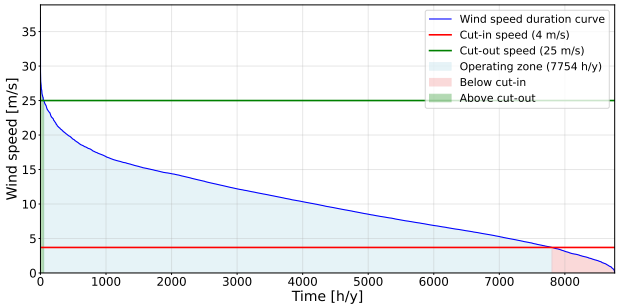

Figure 16: Wind speed duration curve at 80 m height for the Montreal site [9].

To determine the optimal capacity of a wind turbine, the approach began by using a capacity factor ranging from 0 to 1 based on the characteristics of the Vestas V66-1.65 model [10]. This turbine has a rated power of 1.65 MW and was used to estimate the average energy production relative to its full capacity. The optimal installed power required for the project was then calculated to be 1.44 MW.

However, since the V66's nominal power was slightly higher than this optimal value, a second turbine model was chosen: the Vestas V63-1.5 [11]. This turbine has a similar power curve and operating conditions (Figure 17) and its rated power of 1.5 MW is closer to the calculated value. This makes it a more appropriate match, offering similar performance and even a slightly better load factor thanks to its efficiency at lower wind speeds.

Figure 17: Power curves comparison between Vestas V63 and V66 wind turbines.

4.4 Biomass Generation

To produce electricity, biomass is burned in a boiler to generate high-pressure steam. Initially, the energy system design focused on hydroelectricity, and biomass was considered only later as a viable net-zero option. Consequently, the heat and cooling analysis was not conducted using recoverable thermal energy from biomass, but rather through the four-pipe heat pump (4P-HP) system previously described. Moreover, even if heat recovery were implemented, the system would face limitations since the cold demand exceeds the heat demand.

A biomass power plant with an installed capacity of 0.84 MW has been implemented on campus, corresponding to an annual output of 7.4 GWh under full-load operation.

Assuming the use of Miscanthus with a yield of 0.16 GWh/ha/y, this implies a required area of 46 ha under continuous full-load operation. However, given

Table 3: Energy yield for different biomass types [12].

Biomass Resource	Energy Yield
Miscanthus	0.16 GWh/ha/y
Forest Residues	0.01 GWh/ha/y

the actual production of 2.074 GWh/y (corresponding to a capacity factor of 28%), only about 13 ha are effectively needed. Since the total campus area is approximately 500 ha—more than half of which consists of open fields—even the full-load scenario remains entirely feasible in terms of land availability (see Figure 1).

4.5 Solar Photovoltaic

Rooftop surfaces suitable for photovoltaic panels are available across the campus, with the usable area and the corresponding potential installed capacities per district reported in Table 4. Assuming an installation density of 1 kW per 6 m² for PV panels, up to 15.25 MW can potentially be installed across the campus utilizing the 91 500 m² of available rooftops.

A total PV capacity of 1.31 MW is installed. The required area is computed by:

$$S_{Required} = \frac{\dot{W}_{installed}}{U_m \; I_m} \; S_{pannel} \tag{19}$$

Where $\dot{W}_{installed}$ is the installed power of PVs, $S_{required}$ is the surface required for the installed capacity, V_m, I_m and S_{pannel} are respectively the voltage, current and surface of one PV panel.

The required area is therefore approximately 9 100 m^2, making the PV installation highly feasible, as it represents only about 10% of the available rooftop space. For optimal distribution, it is recommended to allocate this area evenly across the four districts within the low-voltage segment of the system. As detailed in Section 5, each district comprises 2 275 m² of rooftop surface area, split between two buildings equipped with PV installations.

To compute the annual PV production shown in Figure 15, the same data source used for the wind analysis was employed [9].

4.6 Pumped Storage

In the western sector of the campus lies a natural lake measuring approximately $200\,\mathrm{m}$ by $210\,\mathrm{m}$, with an average depth of $5\,\mathrm{m}$, corresponding to an estimated volume of about $2.1 \times 10^5\,\mathrm{m}^3$. The lake sits at the campus's lowest point and lies 200 m below the highest elevation, creating favorable conditions for pumped-storage hydroelectric systems. Assuming a hydraulic head of $200\,\mathrm{m}$ and a round-trip efficiency of 0.5, the

Table 4: Available rooftop area and estimated PV capacity (using 6 m²/kW).

District	Dupéré	Hochelaga	Overdale	Anjou	Campus
Available Surface [m²]	22 600	24 700	24 800	19 400	91 500
PV capacity [kW]	3 767	4 117	4 133	3 233	15 250

theoretical storage energy is given by:

$$E = \rho_{\text{water}}\, g\, V\, \Delta h\, \eta \approx 58\,\text{MWh} \qquad (20)$$

The theoretical storage capacity of 58 MWh should be taken as an order of magnitude. The actual capacity of such a construction will be constrained by the area that is available for excavation on the mountain. The maximum capacity has been set to 58 MWh. The upper reservoir will be connected to the nearest point on the transmission grid (TFO) to minimize line costs and landscape impact.

5 Electrical district grid infrastructure

This section presents an optimisation based on a model developped by Franco et al. [13].

5.1 System description

The campus distribution system operates at two nominal voltage levels: Low Voltage (LV) (0.4 kV) and Medium Voltage (MV) (15 kV)[1]. Each of the four districts (*Dupéré*, *Hochelaga*, *Overdale* and *Anjou*) is supplied by a dedicated LV/MV transformer, while inter-district exchanges are routed through the MV network that also connects to the TFO. The five existing substations are characterised by the apparent- power ratings in Table 6.

5.2 Demand and generation data

Every building $b \in \mathcal{B}$ is assigned an hourly active $P^{\text{dem}}_{b,d,t}$ and reactive $Q^{\text{dem}}_{b,d,t}$ demand profile. A PV capacity of 1.31 MW, determined in Section 4, is distributed uniformly across the four districts and dispatched to individual roofs according to available surface area. Additional on-site wind, hydro and biomass installations are aggregated at the *TFO* substation and modelled as the power supplied to the MV network.

Seasonality is captured by three representative days, standing for winter, spring and summer, each resolved into 24 hourly time steps.

5.3 Candidate-grid construction

At the LV level, for each building the three nearest neighbours are defined as candidate interconnection points, forming a grid that is later constrained to radiality by the optimiser.

[1]All quantities are expressed in per-unit unless stated otherwise.

The MV network consist of the shortest paths between district transformers and MV buildings, augmented with a limited set of inter-district links to add flexibility to the optimiser. The LV problems are solved first; net transformer powers $(P^{\text{sup}}_{d,t}, Q^{\text{sup}}_{d,t})$ are then injected as aggregated loads or supplies at the corresponding MV buses.

5.4 Equipment modelling and operational constraints

- Conductors: Two LV and two MV cable technologies are available (Table 5); a binary variable z_{ij} selects at most one conductor per corridor (i, j).
- Substations: Apparent-power limits AS_{max} are obtained by manually decreasing it's value until infeasibility of the problem. (Table 6).
- Storage: A 58 MW h pumped-hydro unit is connected at the TFO (section 4.6). Its state of charge $E_{d,t}$ follows

$$Se_{d,t} = Se_{d,t-1} + \eta\, P^{\text{ch}}_{d,t}\, \Delta t - \frac{1}{\eta} P^{\text{dis}}_{d,t}\, \Delta t, \quad (21)$$

  The state of charge is denoted by E for a given day and time. The charging and discharging powers are represented by P^{ch} and P^{dis}, respectively, while η denotes the efficiency of the conversion process. Daily energy neutrality is ensured by $Se_{d,0} = Se_{d,24}$.
- Reactive support : Shunt capacitors may be installed at LV buses when there is a need to increase the voltage level. The total number is bounded by $\sum_b n_b \leq N_{\text{CAP}}$.
- Operational limits : Kirchhoff's laws, voltage envelopes $V^{min} \leq V_b \leq V^{max}$, line current capacity constraints $I_\ell \leq I^{max}_\ell z_\ell$ and substation ratings are enforced at every time step.

5.5 Optimisation framework

The expansion problem is formulated as a mixed-integer non-linear programme (MINLP). Let $\mathcal{B}$ and $\mathcal{L}$ denote the sets of buses and candidate lines, $\mathcal{S}$ the set of substations, and $\mathcal{T}$ the set of representative time steps. The objective is to minimise the discounted to-

Table 5: Electrical and economic parameters of candidate cables.

Cable	Level	Conductor	Cross-section [mm^2]	R [Ω/km]	X [Ω/km]	I_{max} [A]	Cost [€/km]
2 Al	LV	Al	35	0.512	0.276	150	35 000
4/0 Al	LV	Al	107	0.360	0.205	180	42 000
70 Al	MV	Al	70	0.312	0.154	183	78 000
120 Al	MV	Al	120	0.206	0.116	320	103 000

Table 6: Iteratively derived substation ratings.

	Dupéré	Hochelaga	Overdale	Anjou	TFO
AS_{max} [kVA]	200	100	200	150	10 000

tal cost

$$\begin{aligned} min\ J = K_S\, C_S \sum_{s\in\mathcal{S}} w_s \\ + K_L \sum_{(i,j)\in\mathcal{L}} \ell_{ij}\,(C_{ij}^{\text{line}}\, z_{ij} + \frac{H}{|\mathcal{T}||\mathcal{D}|} C_L\, R_{ij}\, I_{ij}^2) \\ + \sum_{b\in\mathcal{B}} (C_K\, q_b^{\text{bin}} + C_{UN}\, n_b), \end{aligned} \tag{22}$$

where $w_s \in \{0,1\}$ selects substation s, $z_{ij} \in \{0,1\}$ activates one conductor on line (i,j) of length ℓ_{ij} and I_{ij}^2 is the aggregated squared current flowing through that line. Capital-recovery factors K_S and K_L convert investment outlays into equivalent annualised costs. C_S, C_{ij}^{line} and C_L denote respectively the specific substation cost, the conductor-dependent line cost and the energy value. H denotes the total number of hours in a year, while $|\mathcal{T}|$ and $|\mathcal{D}|$ represent the number of time steps per day and the number of representative days, respectively. The fraction $\frac{H}{|\mathcal{T}||\mathcal{D}|}$ serves to scale the computed Joule losses—evaluated over a limited set of hours—to reflect their contribution over the entire year. Finally, q_b^{bin} and n_b are binary and integer variables governing the installation and rating of shunt capacitors at bus b, weighted by their fixed (C_K) and unitary (C_{UN}) costs.

The optimisation is constrained by a power balance, voltage limits, Line current capacity, substation ratings, radial topology and storage dynamics.

5.6 *Economic trade-offs*

The Objective equation (22) embodies the classical trade-off between *capital expenditure* (substations, lines, capacitors) and *operational losses*. The inclusion of binary siting and sizing variables allows the optimiser to weigh infrastructure reinforcement against Joule-loss penalties over the planning horizon, thereby yielding a cost-optimal and technically compliant network design.

5.7 *Optimised layout of the distribution network*

Figure 18 shows the expansion-planning outcome for the four campus districts. Each graph follows the same visual convention:

- **Nodes.** LV buses (individual buildings) are drawn as *circles*, whereas MV buses appear as *pentagons*. A *red square* marks the MV/LV transformer whenever the same building is modelled at both voltage levels. Circles filled in *yellow* host rooftop PV systems, while a *triangle* on a circle indicates that a shunt capacitor has been installed at that LV bus.
- **Lines.** Selected LV cables are plotted in black, while selected MV cables are plotted in blue. MV lines that interconnect districts or link a district to the TFO interface are highlighted in red. Candidate corridors discarded by the optimiser are retained for reference in grey.

The Dupéré district (Figure 18a) contains four LV consumers: B1, B4, B6 and B7, which are fed radially from a single MV/LV transformer located in Building B1. The district is connected directly to the TFO via the B2 bus. The optimiser retained three LV and four MV cables, eliminating most of the grey candidate links. Two LV buses have PV installed on their rooftops. Due to space constraints, the installed capacity is divided as follows: 245.6 kW on B7 and 81.9 kW on B6.

The Hochelaga structure (Figure 18b) is naturally divided into two parts: one with three LV buses connected by two lines and a transformer in the B22 connected to the MV grid; and one with seven MV buses. Due to low demand on the three LV buses, this district sees generation from LV to MV level on sunny days. The installed capacity is divided equally, with 163.75 kW of installed PV on both B24 and B28. B24 is equipped with one 5 kvar shunt capacitors. The district is directly connected to the TFO and also links the following two districts to the TFO generation, as shown by the connection to Anjou. This means that the cables between B21, B29, B25, B27, B26 and B20

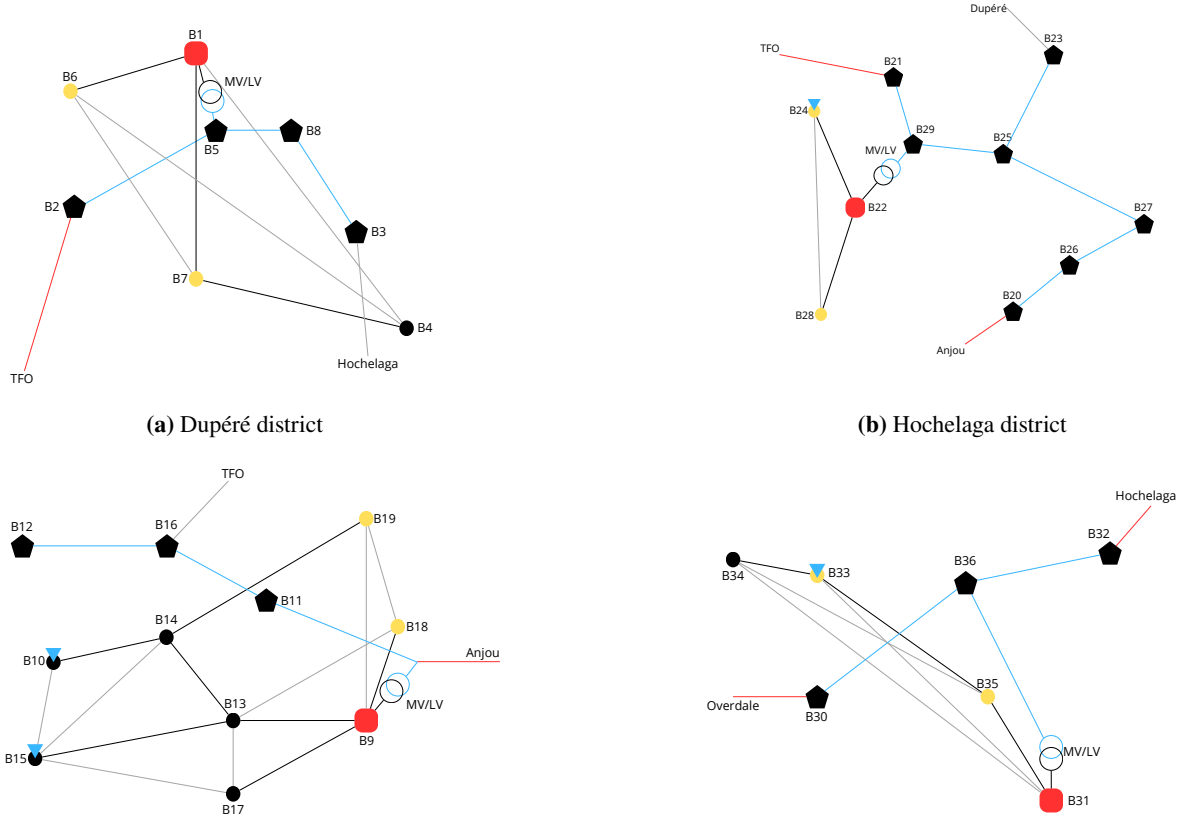

(a) Dupéré district

(b) Hochelaga district

(c) Overdale district

(d) Anjou district

Figure 18: Optimised LV/MV layouts returned by the MINLP.

carry significant power.

With eleven buildings (B9–B19), Overdale (Figure 18c) has the largest LV network. The eight LV buildings are connected radially via seven lines. Two are equipped with shunt capacitors: 14 kvar at B10 and 8 kvar at B15. Two are also equipped with equivalent PV panels, as in Hochelaga. In this district, power comes from the neighbouring district of Anjou and passes through B9, where some of the power goes through the transformer to supply the LV network, while the rest supplies the three MV buses. The optimiser chose to connect to Anjou instead of the TFO, as this district mainly comprises offices, which do not consume as much power as other types of building, such as the hospital in Dupéré. To ensure greater resilience, a backup line could be built between Overdale and the TFO. This backup line would simplify future demand growth by allowing the Anjou-Overdale line to serve as backup while the TFO-Overdale line becomes the primary supply.

Anjou (Figure 18d) serves seven buildings (B30–B36) and is connected to Hochelaga and Overdale. The LV buses are connected in line. Two have equal PV installations and B33 has a 7kvar shunt capacitor.

Across the four districts the optimiser retained:

- 15 LV cables (black) out of 29 candidates, accounting for a distance of 1,550 km, of which 1,425 km are 4/0 Al cables and 125 m are 2 Al. This is probably due to the high power demand during the winter days.
- 17 intra-district MV cables (blue) plus 4 inter-district/TFO links (red), accounting for 4.3 km of 70 Al cables.
- 1.31 MW of PV, evenly divided yet spatially clustered within each district,
- 4 shunt capacitor banks for a total capacity of 34 kvar, all on LV feeders.

The resulting network is strictly radial at both voltage levels and satisfies all voltage, power and current constraints. For a better view of the entire campus, refer to Figure 19, which illustrates the campus electrical network. The line and bus colours have the same meaning as in Figure 18, and the dashed line indicates a backup line.

5.8 Cost assessment

The objective function, represented in Equation (22), provides an equivalent uniform annual cost, account-

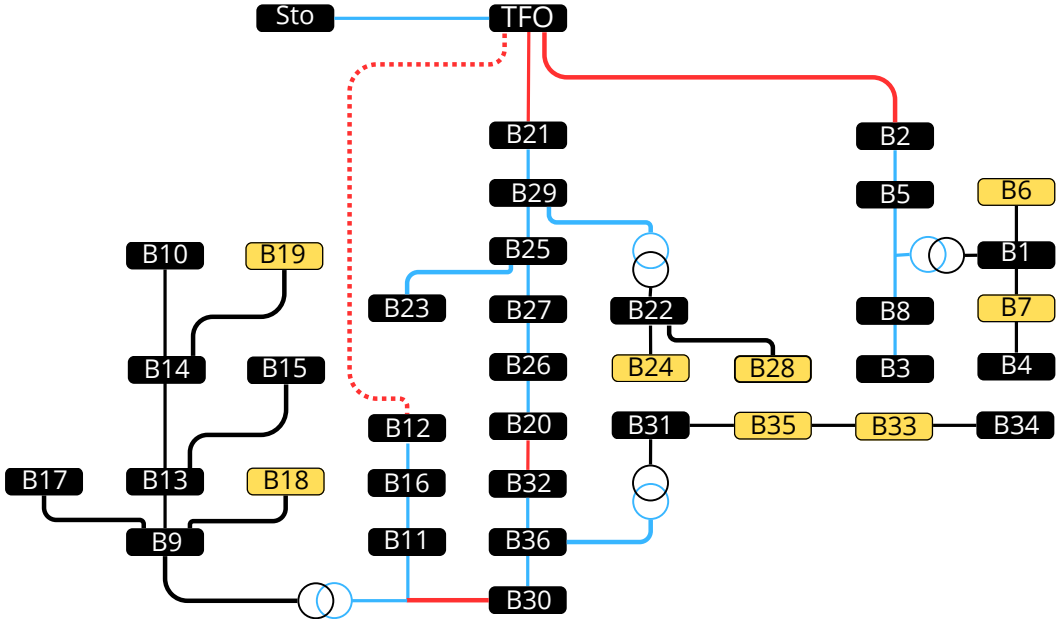

Figure 19: Diagram of the electrical network.

Table 7: Annualised cost of the optimised network $[€/y]$.

	Dupéré	Hochelaga	Overdale	Anjou	MV	Total
Substations	5 200	2 850	6 800	3 900	176 400	195 150
Lines	4 300	1 250	6 000	4 250	27 000	42 800
Capacitors	0	120	440	220	0	780
Total	9 500	4 220	13 240	8 370	203 400	**238 730**

ing for each investment component over a 20-year planning horizon with a discount rate of 5%. The resulting breakdown is presented in Table 7.

The medium-voltage tier (*TFO* column) dominates the expenditure profile, accounting for 85.3 % of the cost. This is mainly driven by the 10 MVA interface transformer, whose annualised cost exceeds the combined LV substation budget by a factor of 9.

Among the LV districts, *Overdale* records the highest annual cost (13.2k€/y) due to a longer set of lines and the additional capacitor bank required for voltage support (cf. Figure 18c).

Line investments represent only 18 % of the overall budget, confirming that the MINLP favoured conductor sizes that minimise lifetime Joule losses rather than bare capital cost.

Reactive-power compensation is negligible in financial terms (<1 %), yet it was necessary to stay in the acceptable voltage range without oversizing conductors.

5.9 Interpretation of the results

The proposed network configuration includes a MV transformers rated at 10 MW to cover a peak load of 3.77 MW, which appears significantly oversized. This over-dimensioning is the main cost driver and likely stems from limitations in the optimizer, which did not allow for smaller transformer capacities, an aspect that could be improved in future iterations. In contrast, LV transformers are more appropriately dimensioned, reflecting the lower demand of LV buildings. The system includes N-1 redundancy at the MV level(except the Dupéré district), enhancing reliability in case of a single failure, while such redundancy is not applied to the LV side, which is acceptable given its lower criticality. Overall, despite the potential for optimization improvements, the solution provides a reliable and scalable infrastructure that addresses the demand requirements effectively.

6 Conclusion

This study assessed the transformation of a conventional campus into a net-zero energy site through a

complete system-level redesign. By integrating local renewable sources—including a 1 MW run-of-river hydro plant, 1.44 MW of wind, 0.84 MW of biomass, and 1.31 MW of PV—the campus achieves a balanced energy mix generating 16.2 GWh annually. Thermal needs are fully met by a centralized 4-pipe heat pump system with a total capacity of 29 modules, delivering 16.3 GWh of heating and cooling services. The total capital cost of the thermal network is approximately 4 M€, with annual operating costs around 458 k€/y. The optimized electrical network infrastructure results in an annualized cost of 240 k€/y. These figures confirm the technical feasibility and economic viability of achieving a carbon-neutral, fully self-sufficient campus in Montreal.

References

[1] C. L. Kwan and A. Hoffmann, "Chapter 27 - the los angeles community college district: Establishing a net zero energy campus", in *Sustainable Cities and Communities Design Handbook Green Engineering, Architecture, and Technology*, Oxford, United Kingdom: Butterworth-Heinemann, 2018, pp. 537–556.

[2] R. Annette, E. Ursula, S.-E. Karin, L. Rüdiger, and W. Verena, "Net zero energy strategies and planning support tools for campuses and residential neighborhoods in germany", *ASHRAE Transactions*, vol. 126, 2020.

[3] J. M. Rey-Hernández, F. J. Rey-Martínez, C. Yousif, and D. Krawczyk, "Assessing the performance of a renewable district heating system to achieve nearly zero-energy status in renovated university campuses: A case study for spain", *Energy Conversion and Management*, vol. 292, 2023.

[4] *University of minnesota morris*, Section : Sustainability Goals Initiatives. [Online]. Available: https://morris.umn.edu/sustainability-umn-morris/sustainability-goals-initiatives.

[5] ULiège, *Le campus du sart tilman chauffé grâce à la cogénération biomasse*. [Online]. Available: https://www.durable.uliege.be/cms/c_10382858/fr/le-campus-du-sart-tilman-chauffe-grace-a-la-cogeneration-biomasse#:~:text=La%20cog%C3%A9n%C3%A9ration%20biomasse%20est%20int%C3%A9gr%C3%A9e,deux%20silos%20de%20200%20m%C2%B3..

[6] FläktGroup, *Data sheet : 4-pipe heat pump heamo air*, Modele 8080. [Online]. Available: https://www.flaktgroup.com/es/products/air-conditioning-heating/chillers-and-heat-pumps/air-cooled-chillers-and-air-to-water-heat-pumps/air-to-water-heat-pumps-for-simultaneous-cooling-and-heating-4-pipe-units/fgas-4034-8080-eg2-r454b-334-779kw/.

[7] *Electricity maps*. [Online]. Available: https://app.electricitymaps.com/zone/CA-QC/72h/hourly.

[8] Creseb, *Débit minimum biologique (dmb) et gestion quantitative de la ressource en eau*. [Online]. Available: https://www.creseb.fr/voy_content/uploads/2015/11/dmb-gestion-quantitative-ressource-en-eau_guide_creseb_2015.pdf.

[9] S. Pfenninger and I. Staffell, *Renewables.ninja*. [Online]. Available: https://www.renewables.ninja/.

[10] L. Bauer and S. Matysik, *Le grand portail de l'énergie éolienne*, 2011-2025. [Online]. Available: https://fr.wind-turbine-models.com/turbines/15-vestas-v66-1.65.

[11] L. Bauer and S. Matysik, *Le grand portail de l'énergie éolienne*, 2011-2025. [Online]. Available: https://fr.wind-turbine-models.com/turbines/821-vestas-v63.

[12] P. Dewallef, *Lecture 09: The Biomass Ressource and Conversion*. 2024-2025, p. 8.

[13] J. F. Franco, M. J. Rider, and R. Romero, "A mixed-integer quadratically-constrained programming model for the distribution system expansion planning", *Int. J. Elect. Power Energy Syst.*, vol. vol. 62, Nov. 2014.

[14] M. Hampshire-Waugh, *Energy supply, power density, and land use*, 2023. [Online]. Available: https://net-zero.blog/book-blog/land-use-by-energy-source.

Appendix

Table 8: Input Parameters for Centralized Heating and Cooling Pipe Design.

Symbol	Heating	Cooling	Unit	Description
L	7.6	7.6	[km]	Length of the pipe
ε	1×10^{-5}	1×10^{-5}	[m]	Pipe roughness
e	0.12	0.12	[m]	Insulation thickness
k_{in}	0.03	0.03	[W/m K]	Thermal conductivity of insulation
d	2	2	[m]	Pipe burial depth
k_{gr}	2	2	[W/m K]	Thermal conductivity of surrounding ground
$\dot{W}_{max}$	5000	5600	[kW]	Maximum thermal power capacity
E_{tot}	4150	12000	[MWh]	Annual transported thermal energy
ΔT	5	5	[°C]	Temperature difference between supply and return
T_{su}	45	7	[°C]	Supply temperature
T_{amb}	7	7	[°C]	Ambient ground temperature
Y_{elec}	51	51	[€/MWh]	Electricity price
$Y_{heat/cold}$	60	94	[€/MWh]	Market reference price for heat or cold

Table 9: Input data per stage used for EES modeling (fl = full load).

Parameter	Symbol	Value
Cooling capacity (fl)	$\dot{Q}_{ev}$	201.8 [kW]
Heating output (fl)	$\dot{Q}_{cd}$	257.5 [kW]
Power consumption (fl)	$\dot{W}_{ch}$	60.45 [kW]
Thermal Efficiency Ratio	TER	7.6 [-]
Chilled water outlet T	$T_{w,ev,ex}$	7 [°C]
Hot water outlet T	$T_{w,ex,cd}$	45 [°C]
Refrigerant type	'fluid$'	R-454B
Chilled water $\dot{m}$	$\dot{m}_{w,ev}$	5.67 [kg/s]
Hot water $\dot{m}$	$\dot{m}_{w,cd}$	16.32 [kg/s]
Number of compressor	N_{cp}	2 [-]
Chilled water inlet T	$T_{c,su,ev}$	12 [°C]
Hot water inlet T	$T_{w,su,cd}$	40 [°C]
Fan power consumption	$\dot{W}_{fan}$	4×2.7 [kW]

Participation

Cabay Raphaël :

During the first quarter, the workload was split evenly between us, at about 25% each. My share covered the literature review, field-constraint mapping, data analysis, the initial energy-mix scenarios and a preliminary electrical grid model. Some of these were revised in Q2.

During the second quarter, I participated in the decision-making process regarding centralized, decentralized and hybrid thermal system, rebuilt the energy mix model for the Energy Transition course and produced the optimisation framework for the electrical grid.

Finally, I wrote the entire final report with Maxime.

Haas Maxime :

During the first quadrimester, all team members contributed equally to the project, each investing approximately 25% of their effort. I specifically concentrated on the electrical and thermal mix analyses, with the electrical mix component being partially redesigned in the second quadrimester.

During the second quadrimester, I participated in the decision-making process regarding centralized, decentralized and hybrid systems (which has not been developed in this report). Then I designed the full centralized pipe network. Following this decision, I collaborated with a team member from the University of Brussels to develop the EES code. We implemented the code together. I integrated the heating and cooling demand data into the model. Finally, by adapting the code with our specific data, I was able to extract the annual TER for the entire district.

Finally, I wrote the entire final report with Raphael.

Werbrouck Alexis :

During the first quarter, the workload was split evenly, around 25 % each. My contributions included the literature review, field-constraint mapping, data analysis, drafting the initial energy-mix scenarios, and creating a preliminary electrical-grid model, several of which were refined in Q2.

In the second quarter, I participate in the energy-mix model and took charge of gathering and organizing the data needed for the electrical-network analysis.

I do the data gathering in the cours "Energy transition".

O.Hamad Ishak :

During the first quarter, the workload was split evenly between us, at about 25% each. I focused on conducting a literature review, identifying field constraints, analysing data, outlining the initial energy mix options and setting up a prototype electrical grid model. Many of these tasks were revisited later.

During the second quarter, I collaborated on revising the energy mix assessment and on the search of the datasets for the electrical network.